ISBN: 978-3-95450-227-1 ISSN: 2673-5490 doi:10.18429/JACoW-IPAC2022-WEPOMS004

INVESTIGATION OF RF HEATING FOR THE MULTIPOLE INJECTION KICKER INSTALLED AT SOLEIL

A. Gamelin*, P. Alexandre, R. Ben El Fekih, J. Da Silva Castro, M. El Ajjouri, A. Letresor, L. S. Nadolski, R. Ollier, S. Thoraud, Synchrotron SOLEIL, Gif-sur-Yvette, France
M. Sacko, S. Taurines, Avantis Concept, Saint-Cere, France

Abstract

During the commissioning of the new Multipole Injection Kicker (MIK) pulsed magnet at SOLEIL synchrotron, an anomalously high heating of the MIK chamber and flanges was found. To better manage the heat load, fans directed toward the MIK were added to improve the air-cooling flow. This allowed the nominal current to be reached in all operation modes while keeping reasonable temperatures on the MIK. Post-installation investigations subsequently showed that the initial estimate of the maximal heat load was in agreement with the measured temperature in several operation modes both with and without the additional fans. In this article, we present the complete study, starting from the impedance calculation to thermal simulations, and comparison with the measured data with beam.

MULTIPOLE INJECTION KICKER

Non-linear kicker magnets, such as the Multipole Injection Kicker (MIK), are key components for compact injection scheme of some 4th generation light sources [1, 2]. Non-linear kicker magnets are pulsed magnets characterized by an off axis field region where the injected beam is located and a field free region on the stored beam path. They are developing since their first use at KEK-PF [3] and BESSY II [4] as they allow for different types of on-axis and off-axis injections types in rings with small dynamic aperture [2]. The MIK provides a combined quadrupolar and octupolar pulsed field which allows for a near-transparent injection compared to the usual bump-based scheme using several kickers [1].

The MIK, designed and built by SOLEIL in collaboration with MAX IV, is composed of a racetrack chamber made of monocrystaline sapphire where grooves are precisely machined to hold copper conductors in the direction parallel to beam propagation, see Fig. 1. The inside of the chamber is coated with titanium to shield the beam from the sapphire body, allowing the image current to flow over the titanium layer and reducing the thermal load. But the coating thickness can not be too large as it induces a disturbance of the magnetic field and generates a pulsed quadrupolar component via eddy currents [5]. A compromise must therefore be found on the coating thickness to get a magnet with good performance with a contained thermal load.

A first prototype of the MIK was installed at MAX IV 3 GeV ring in 2017 where heating due to the 0.8 µm thin titanium coating was found to be an issue [1]. The problem was solved in 2019 when an improved chamber with a thicker coating of 3.5 µm was installed. The MIK is now routinely used for day to day operation at MAX IV with excellent performance [1].

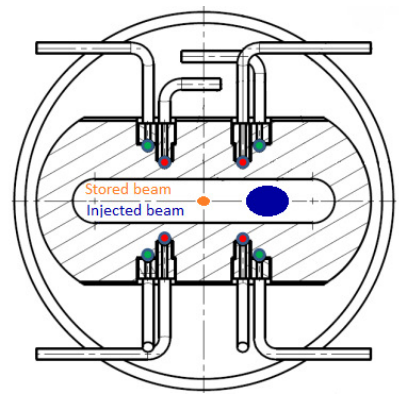

Figure 1: Cross section of the MIK showing the position of the copper conductors (red and green dots), the injected and stored beam.

Another MIK device was installed in the 2.75 GeV storage ring of SOLEIL in January 2021 and is being commissioned [6–8]. As the SOLEIL MIK also presents anomalously high temperatures, a post-installation investigation was initiated to review the RF heating estimate, the choice of the coating thickness and understand the observed high temperatures. This article describes the findings from this investigation and presents the different components: impedance calculations, temperature measurements with beam and thermal simulations.

IMPEDANCE CALCULATIONS

The impedance calculations shown here for the MIK chamber and flanges, the two elements where significant heating is observed, were performed prior to installation and are based on the MIK mechanical design that is described in detail in [9].

MIK Chamber

The MIK is composed of a single 33 cm long racetrack chamber with an inner aperture of 46.8 mm in horizontal and 7.8 mm in vertical plane. Its geometric (longitudinal) impedance is thus negligible compared to the resistive wall one produced by the titanium coating deposited on the sapphire body.

The coating thickness was measured at 3.5 µm using control pellets used during the deposit. The DC resistance of

* alexis.gamelin@synchrotron-soleil.fr

Content from this work may be used under the terms of the CC BY 4.0 licence (© 2022). Any distribution of this work must maintain attribution to the author(s), title of the work, publisher, and DOI

ISBN: 978-3-95450-227-1 ISSN: 2673-5490 doi:10.18429/JACoW-IPAC2022-WEPOMS004

Content from this work may be used under the terms of the CC BY 4.0 licence (© 2022). Any distribution of this work must maintain attribution to the author(s), title of the work, publisher, and DOI
This is a preprint — the final version is published with IOP

the coating was also measured at 3.43 Ω using the two probe method. From this measurement, assuming that the coating is homogeneous, its resistivity can be estimated between 2.83×10^{-6} Ω m and 3.73×10^{-6} Ω m depending whether the deposition is considered to be present only on the horizontal sections or on the whole chamber.

The measured resistivity value of the coating is quite different from the usual titanium resistivity in its metallic form: 4.27×10^{-7} Ω m. The reason for this difference could be related to the sputtering method used to realize the titanium deposition, leading to an amorphous structure of the titanium, more resistive than the usual metallic form.

The resistive wall impedance of the MIK chamber can then be computed using the multi-layered flat chamber analytic model implemented in the `ImpedanceWake2D` code [10, 11] or, neglecting the effect of the high relative permittivity ϵ_r of the sapphire body, using Eq. (5) of [12]. Input values for the `ImpedanceWake2D` code are shown in Table 1.

Table 1: Input Values for `ImpedanceWake2D` Code for the "Amorphous Titanium" MIK Chamber Model

Layer	Thickness	DC resistivity	ϵ_r
Vacuum	3.9 mm	∞	1
Titanium	3.5 µm	3×10^{-6} Ω m	1
Sapphire	11.1 mm	1×10^{12} Ω m	10 (≈ 9.3/11.5)
Vacuum	∞	∞	1

The real part of the longitudinal impedance obtained using both methods is shown in Fig. 2 for both an "amorphous titanium" layer using the measured resistivity and a metallic layer. The good agreement between both methods shows that the 3.5 µm titanium coating effectively shields the beam from the sapphire high relative permittivity and poor conductivity. In uniform filling at 500 mA (416 bunches), with the measured bunch length of 19.8 ps, the expected thermal load of each model yields 112 W for the "amorphous titanium" impedance and 17 W for the metallic titanium one.

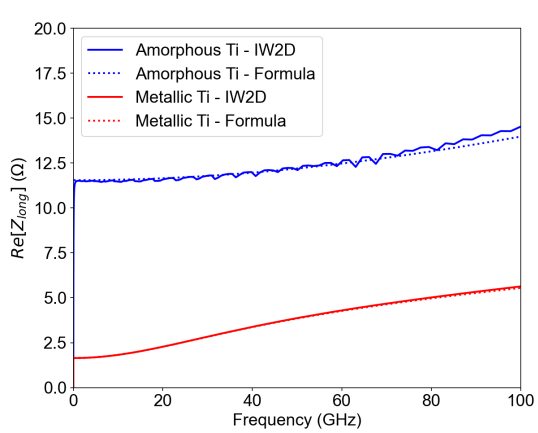

Figure 2: Real part of the longitudinal impedance of the MIK chamber.

At SOLEIL, the highest thermal stress comes from the 8 bunch filling pattern where a total current of 110 mA is stored. For this mode, the expected thermal load was about 156 W for a maximum power density of 3.6 W mm^{-2} in the center of the MIK chamber. This power density was estimated to be low compared to the one generated by synchrotron radiation in near by areas so a thermal simulation was deemed unnecessary at the time.

MIK flanges

The junction between the MIK chamber and its flanges is ensured by a brazed sapphire/copper interface, then a brazed copper/stainless steel interface and finally a stainless steel/flange weld [9]. The flanges are made of 316L stainless steel and have the same racetrack cross section as the MIK chamber. The flanges also integrate small bellows shielded from the beam by RF fingers. The flange vertical aperture increases locally from the 8 mm of the MIK to 9 mm at the RF fingers location to decrease again to 8 mm at the upstream/downstream connection with taper-absorber elements. The small cavity created by this aperture variation leads to two trapped modes at 16.7 GHz and 19.2 GHz with a corresponding amplitude of 247 Ω and 40 Ω in the longitudinal impedance spectrum.

For the uniform filling mode at 500 mA and for full coincidence with beam spectrum line, the power deposited by the first mode was estimated to be around 2.8 W for a maximum power density of 0.5 W mm^{-2}. The resistive wall heating for the same operation mode was evaluated around 2.0 W for a maximum power density of 0.4 W mm^{-2}.These flanges were designed to accommodate the MIK aperture to the cross-section of the SOLEIL straight section. Considering the lack of timely fallback solutions, it was decided to keep this design despite the trapped mode, as the expected heat load was low and there was no danger of coupled bunch instabilities.

BEAM MEASUREMENTS

After the MIK installation, significant heating was measured at the downstream extremity of the MIK chamber where the temperature reached 130 °C for a beam current of 300 mA. To contain the temperature rise and allow the nominal current to be reached in all operation modes, the following steps had to be taken: the MIK outer frame was removed, two heatsinks were installed on the MIK chamber body and three fans directed toward the MIK were used to improve the air-cooling flow.

As the heat load was not linearly proportional to the stored current, the synchrotron radiation was quickly ruled out as a potential contributor. Temperature sensors installed on the MIK and thermal camera measurements made right after a beam dump then shown a asymmetry between the upstream and downstream regions of the MIK. In addition to data taken in the different user operation modes, additional measurements were taken with the fans off during a dedicated machine development shift. The two observed cases were

ISBN: 978-3-95450-227-1 ISSN: 2673-5490 doi:10.18429/JACoW-IPAC2022-WEPOMS004

selected to mimic the usual operation modes parameters, in particular bunch length, but with an overall lower beam current in order not to overheat the MIK. Measured data is compared to simulated data in Table 2.

THERMAL SIMULATIONS

The thermal simulation was performed following the methodology described in [13, 14]. Firstly, 3D maps of the dissipated power were generated at different frequencies (DC for the resistive wall, mode frequencies for the geometric impedance) using CST wakefield solver [15]. Then these maps were re-scaled using the deposited power computed at that frequency using the beam properties and impedance as input. After this procedure, the different power maps corresponding to each operation modes can be used as input in a thermomechanical simulation software like ANSYS [16] and mapped to the 3D geometry.

For the thermal simulation, convection was imposed on all MIK surfaces exposed to air with an heat transfer coefficient of 5 $W\,m^{-2}\,K^{-1}$ when the fans where off (free convection) and of 46.2 $W\,m^{-2}\,K^{-1}$ when they were switched on (forced convection). The value for the heat transfer coefficient with fans was computed by taking into account airflow rate of the fans and the MIK chamber geometry.

The simulated temperatures on the MIK chamber are compared to those measured in the upstream and downstream regions in Table 2. The range of measured values correspond to 4 measurement points in the upstream region (2 of them providing too low values were discarded as outliers, maybe because of a weak thermal contact with the MIK chamber) and 5 measurement points in the downstream region. The simulated value reported corresponds to the maximum value but the simulated temperature distribution is very homogeneous (a few °C of difference at maximum) as the heat is due to the resistive wall.

When the fans are turned off, the temperature spread along the different measurement points is much more limited than when the fans are switched on as the fans air flow is not uniform on the MIK body. There is a good match between the simulated temperatures and the ones measured in the upstream region for all cases. It seems to indicate that the impedance model, using measured resistivity, and the methodology is correct. But the measured temperatures in the downstream region are consistently higher than in the upstream one and therefore do not match with the simulation.

Two possible hypotheses were advanced to explain the abnormal heating observed in the downstream region: a local degradation of the titanium coating or a partial loss of the RF contact on the neighbouring flange.

The flanges were simulated with the same method but in this case the temperature rise is very moderate because the total deposited power is lower than 5 W for the worst case. The extreme case of no RF contact has also been simulated but gives much too high temperatures due to the huge deposited power (1.6 kW for the worst case). The measured temperatures on the downstream flange are always lower than the those measured on the downstream MIK region, e.g. 75 °C for the 100 mA case and 115 °C for the 25 mA case. So it seems that the most probable explanation is a local degradation of the coating.

When the MIK and its flanges are simulated together with perfect thermal contact, the simulated temperature on the MIK decreases a bit for the case without fans, from 10 °C to 20 °C, compared to Table 2 as some of the heat is transferred in the flanges. This transfer is expected and can explain the high temperatures at the downstream flange if the coating is degraded in that very region. The temperature drop on the MIK chamber compared to Table 2 could either indicate that the coating resistivity is underestimated or more likely that the perfect thermal contact hypothesis is too coarse and that a refined model using an experimental thermal contact conductance should be used [17]. The thermal simulation performed with ANSYS was also benchmarked against CST Conjugate Heat Transfer (CHT) solver and gave similar results.

CONCLUSION

This investigation showed that the initial thermal load estimate using the measured resistivity was correct but that its consequence were underestimated. The imbalance between the upstream and downstream region still need to be better understood and a future visual inspection of the MIK during a machine shutdown could help in this respect.

Future MIK devices could be improved on this aspect by using thermal simulation during the design phase to optimize the heat transfer and integrate cooling fans in the base design. The heat amount could also be reduced by a slight increase of the coating thickness, but at the cost of increased field perturbations.

Table 2: Comparison between the Simulated and Measured Temperatures of the MIK Chamber

Current	Filling mode	Fans	Simulated	Upstream	Downstream
500 mA	Uniform (416 bunches)	On	61 °C	52 °C to 69 °C	86 °C to 125 °C
500 mA	Uniform (416 bunches)	Off	335 °C		
110 mA	8 bunches	On	72 °C	64 °C to 74 °C	113 °C to 164 °C
110 mA	8 bunches	Off	425 °C		
100 mA	1/4 (104 bunches)	Off	72 °C	69 °C to 72 °C	85 °C to 86 °C
25 mA	2 bunches	Off	107 °C	103 °C to 112 °C	136 °C to 138 °C

Content from this work may be used under the terms of the CC BY 4.0 licence (© 2022). Any distribution of this work must maintain attribution to the author(s), title of the work, publisher, and DOI

ISBN: 978-3-95450-227-1 ISSN: 2673-5490 doi:10.18429/JACoW-IPAC2022-WEPOMS004

Content from this work may be used under the terms of the CC BY 4.0 licence (© 2022). Any distribution of this work must maintain attribution to the author(s), title of the work, publisher, and DOI

REFERENCES

[1] P. Alexandre *et al.*, "Transparent top-up injection into a fourth-generation storage ring," *Nucl. Instrum. Methods Phys. Res., Sect. A*, vol. 986, p. 164 739, 2021. doi:10.1016/j.nima.2020.164739.

[2] M.-A. Tordeux *et al.*, "Injection Schemes for the SOLEIL Upgrade," in *Proc. IPAC'21*, Campinas, Brazil, May 2021, pp. 796–798. doi:10.18429/JACoW-IPAC2021-MOPAB248.

[3] H. Takaki *et al.*, "Beam injection with a pulsed sextupole magnet in an electron storage ring," *Phys. Rev. Spec. Top. Accel Beams*, vol. 13, no. 2, p. 020 705, 2010.

[4] O. Dressler, T. Atkinson, M. Dirsat, P. Kuske, and H. Rast, "Development of a Non-Linear Kicker System to Facilitate a New Injection Scheme for the BESSY II Storage Ring," in *Proc. IPAC'11*, San Sebastian, Spain, Sep. 2011, pp. 3394–3396.

[5] J. Kallestrup *et al.*, "Studying the Dynamic Influence on the Stored Beam From a Coating in a Multipole Injection Kicker," in *Proc. IPAC'19*, Melbourne, Australia, May 2019, pp. 1547–1550. doi:10.18429/JACoW-IPAC2019-TUPGW063.

[6] R. Ollier, P. Alexandre, R. B. E. Fekih, and L. S. Nadolski, "Design and Commissioning of a Multipole Injection Kicker for the SOLEIL Storage Ring," in *Proc. IPAC'21*, Campinas, Brazil, May 2021, pp. 3525–3528. doi:0.18429/JACoW-IPAC2021-WEPAB353.

[7] L. S. Nadolski *et al.*, "SOLEIL Update Status," in *Proc. IPAC'21*, Campinas, Brazil, May 2021, pp. 3945–3948. doi:10.18429/JACoW-IPAC2021-THPAB078.

[8] R. Ollier *et al.*, "Performance Report of the SOLEIL Multipole Injection Kicker," presented at IPAC'22, Bangkok, Thailand, Jun. 2022, paper THPOPT039, this conference.

[9] J. D. S. Castro, P. Alexandre, R. B. E. Fekih, and T. S. Thoraud, "Multipole Injection Kicker (MIK), a Cooperative Project SOLEIL and MAX IV," in *Proc. MEDSI'18*, Paris, France, Jun. 2018, pp. 48–49. doi:10.18429/JACoW-MEDSI2018-TUPH12.

[10] N. Mounet and E. Métral, "Impedances of Two Dimensional Multilayer Cylindrical and Flat Chambers in the Non-Ultrarelativistic Case," in *Proc. HB'10*, Morschach, Switzerland, Sep.-Oct. 2010, pp. 353–357.

[11] N. Mounet, *ImpedanceWake2d*.

[12] M. Migliorati, E. Belli, and M. Zobov, "Impact of the resistive wall impedance on beam dynamics in the future circular e+ e- collider," *Phys. Rev. Accel. Beams*, vol. 21, no. 4, p. 041 001, 2018.

[13] L. Teofili, M. Migliorati, D. C. Perez, F. Giordano, I. L. Garcia, and G. Mazzacano, "A Multi-Physics Approach to Simulate the RF Heating 3D Power Map Induced by the Proton Beam in a Beam Intercepting Device," in *Proc. IPAC'18*, Vancouver, Canada, Apr.-May 2018, pp. 3452–3455. doi:10.18429/JACoW-IPAC2018-THPAK093.

[14] L. Teofili, "A thermomechanical and electromagnetic approach for the design of high-intensity accelerator components," Ph.D. dissertation, Roma La Sapienza, 2019.

[15] *CST studio suite 3D EM simulation and analysis software*. www.cst.com

[16] *ANSYS*. www.ansys.com

[17] L. V. Cid, A. Abánades, M. Barnes, F. Mostchmann, V. Vlachodimitropoulos, and W. Weterings, "Conception and design of a cooling system for the lhc injection kicker magnets," *Nucl. Instrum. Methods Phys. Res., Sect. A*, vol. 916, pp. 296–305, 2019. doi:10.1016/j.nima.2018.11.007